Room Temperature Magnetic Order in Air-Stable

Ultra-Thin Iron Oxide

Jiangtan Yuan¹†, Andrew Balk²†, Hua Guo¹, Qiyi Fang¹, Sahil Patel¹, Xuanhan Zhao³, Tanguy Terlier⁴, Douglas Natelson³, Scott Crooker², Jun Lou¹*

ABSTRACT

Manual assembly of atomically thin materials into heterostructures with desirable electronic properties is an approach that holds great promise. Despite the rapid expansion of the family of ultra-thin materials, stackable and stable ferro/ferri magnets that are functional at room temperature are still out of reach. We report the growth of air-stable, transferable ultra-thin iron oxide crystals that exhibit magnetic order at room temperature. These crystals require no passivation and can be prepared by scalable and cost-effective chemical vapor deposition. We demonstrate that the bonding between iron oxide and its growth substrate is van der Waals-like, enabling us to remove the crystals from their growth substrate and prepare iron oxide/graphene heterostructures.

¹ Department of Materials Science and NanoEngineering, Rice University, Houston, TX 77005, USA

² National High Magnetic Field Laboratory, Los Alamos, New Mexico 87545, USA

³ Department of Physics and Astronomy, Rice University, Houston, TX 77005, USA

⁴ Shared Equipment Authority, Rice University, Houston, TX 77005, USA

KEYWORDS: iron oxide, room temperature magnetism, van der Waals heterostructure, ultra-thin

There is great interest in using mechanical stacking¹⁻², rather than epitaxial materials growth, to assemble heterostructures of materials which exhibit diverse, intriguing properties such as valley polarization³, ferroelectricity⁴, superconductivity⁵ and charge-density waves⁶⁻⁷. Efforts have been made to create stackable magnetic materials through engineering of defects, but only local magnetism has been achieved⁸⁻¹⁰. The recent discoveries of layered materials supporting intrinsic ferromagnetism have made stacked spintronic heterostructures realistic 11-17. However, manual assembly of multilayer devices with these ferromagnets under ambient conditions remains challenging due to material sensitivity to environmental degradation, and magnetic order at room temperature is rare in van der Waals materials. Here, we show synthesis of ultra-thin crystals of ε-Fe₂O₃ with scalable ambient pressure chemical vapor deposition (CVD), finding ready formation on both silicon and mica substrates. Electron microscopy and Raman spectroscopy measurements confirm that the crystals are pure ε-Fe₂O₃, with no detectable amounts of the more common α-Fe₂O₃ and γ-Fe₂O₃, for crystals thinner than approximately 100 nm. Furthermore, magneto-optical Kerr effect (MOKE) magnetometry of individual crystals show that they are magnetically stable, with coercive fields of hundreds of mT. We observe robust hysteresis even in crystals as thin as 7 nm at room temperature in atmosphere. These samples of ultra-thin ε-Fe₂O₃ can be readily transferred from growth substrates in aqueous solutions at ambient conditions to arbitrary substrates without any visible structural changes. Finally, despite the fact that these CVD-grown ultra-thin ε-Fe₂O₃ crystals are not van der Waals materials, their atomically sharp surfaces and nanoscale thicknesses allow them to be easily integrated with 2D materials such as graphene, thereby eliminating the lattice mismatching constraints for design of

functional heterostructures. This CVD growth, manipulation, and magnetic study of comparatively large individual crystals is complementary to recent successes in liquid-phase exfoliation of ensembles of nanoscale ultrathin hematite crystals¹⁸.

ε-Fe₂O₃ has an orthorhombic structure with lattice constants a = 5.072 Å, b = 8.736 Å, c = 9.418 Å and belongs to the space group of $Pna2_1$. There are four independent crystallographically nonequivalent iron sites, denoted as Fe_A, Fe_B, Fe_C and Fe_D, occupying the center of either the octahedron or tetrahedron formed by surrounding oxygen atoms (Fig. 1a). We grow samples with standard CVD techniques (see Methods for growth details in SI). Ultra-thin crystals of iron oxide with lateral size of ≈10 μm readily form using this procedure, and are apparent in optical micrographs (Fig. 1b-d). All crystals exhibit well-defined shapes with sharp edges, showing clear evidence of high crystallinity.

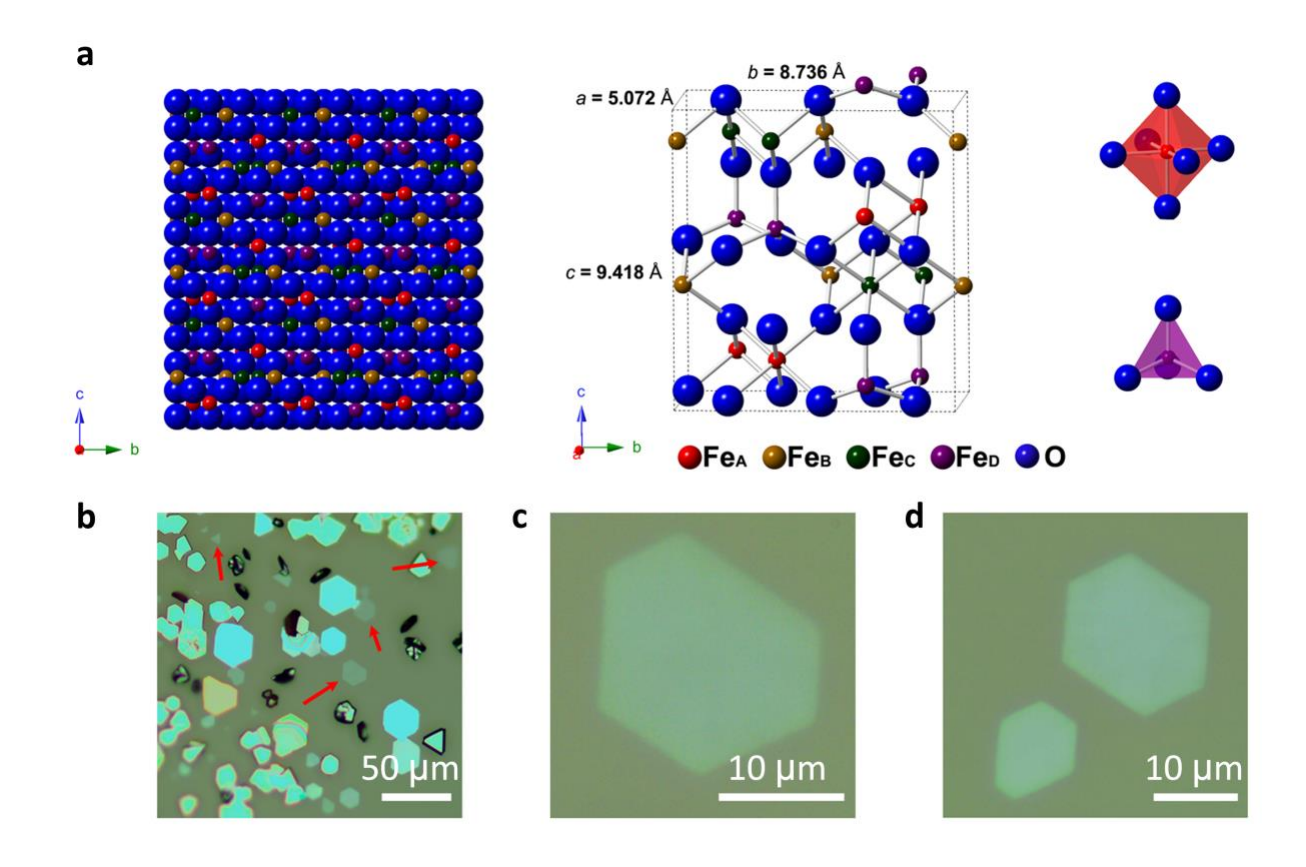


Figure 1. Crystal structure and optical images of ε-Fe₂O₃. (a) Non-layered ε-Fe₂O₃ has an orthorhombic structure with a = 5.072 Å, b = 8.736 Å and c = 9.418 Å. There are four independent iron sites, denoted as Fe_A, Fe_B, Fe_C and Fe_D. Inset: Individual octahedron formed by one center iron atom and six surrounding oxygen atoms, representing the cation coordination of Fe_A, Fe_B, Fe_C, and an individual tetrahedron formed by one center iron atom and four surrounding oxygen atoms, representing the cation coordination of Fe_D. (b-d) Optical images of ε-Fe₂O₃ crystals grown on mica by CVD. Ultra-thin crystals with a lateral size of many μm can be easily found in each batch of growth, as indicated by the red arrows. The out-of-plane growth direction is [001]. Grain structure of the crystals is discussed below.

Figure 2a and 2b are atomic force microscopy (AFM) images of two representative crystals with thicknesses of \approx 5.8 nm and \approx 7.5 nm (Fig. 2c, d). The thinnest crystal we have measured is \approx 5.1 nm which is only five unit-cells thick. The ultra-thin Fe₂O₃ crystals have atomically smooth surfaces and uniform thicknesses, with standard deviation roughness less than 0.5 nm. Micro-Raman measurements of these samples (Fig. 2g) shows four peaks between 100 cm⁻¹ and 200 cm⁻¹, which are the characteristic first-order phonon vibration modes M1-M4 of ϵ -Fe₂O₃, in agreement with previous literature²⁰. In comparison, the most stable bulk phase α -Fe₂O₃ has no Raman active modes in this range. Full spectra comparison can be found in Fig. S1. Spatially resolved Raman mappings (Fig. 2e, f) further suggest uniformity within individual crystals. No detectable second phase was observed.

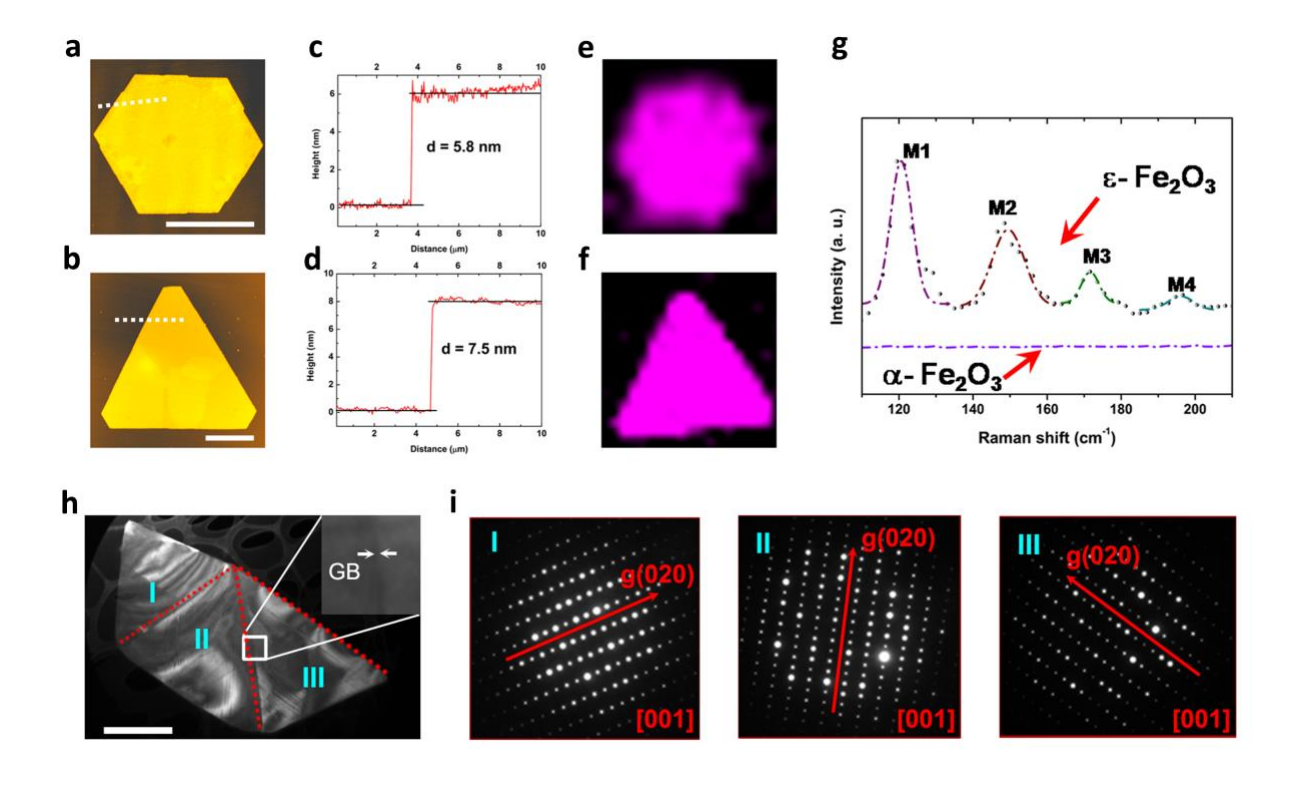


Figure 2. Characterization of ε-Fe₂O₃. (a) (b) Two representative ultra-thin ε-Fe₂O₃ crystals with hexagonal and triangular shapes grown on a mica substrate. The well-defined shapes indicate high crystal quality. Scale bars are 5 μm. (c) (d) AFM thickness measurements for crystals in (a), (b). The thicknesses are 5.8 nm and 7.5 nm, respectively. (e) (f) The corresponding spatially resolved Raman mapping for crystals in (a) and (b). The intensities are the sum of signals between 100 cm⁻¹ and 200 cm⁻¹, normalized by Raman peak of mica substrate. The homogeneous intensity distributions show that ε-Fe₂O₃ phase is uniformly distributed within the crystals. (g) Raman spectra collected from ε-Fe₂O₃ and α-Fe₂O₃ crystals on silicon oxide. The four characteristic peaks between 100 cm⁻¹ and 200 cm⁻¹ represent the first-order phonon modes, namely M1-M4, of ε-Fe₂O₃, whereas α-Fe₂O₃ has no active Raman modes in this range. Peaks are fitted by Lorentz functions. (h) Dark-field TEM image of an ultra-thin ε-Fe₂O₃ polycrystalline flake transferred from mica substrate. At least three individual grains, marked by I, II and III are present in this flake.

GBs are highlighted by red dotted lines. Inset: Zoom-in image of a GB. (i) Electron diffraction patterns from three grains in (h), which can also be indexed to the orthorhombic symmetry of ε -Fe₂O₃ in the [001] zone axis. The angles between grain I and II, and grain II and III are about 56° and 45°, respectively.

We employed transmission electron microscopy (TEM) to gain further structural insight of the as-synthesized ultra-thin Fe₂O₃. Fig. 2h is a dark-field TEM image of an ultra-thin Fe₂O₃ polycrystalline flake where grain boundaries (GBs) can be visualized. The GBs are highlighted by red dotted lines and a zoom-in GB is displayed in the inset of Fig. 2h. At least three grains, marked by I, II and III, are present in this flake. The electron diffraction patterns (Fig. 2i) from a randomly selected area in each grain can be indexed to the orthorhombic symmetry of ε-Fe₂O₃ in the [001] zone axis, consistent with the results from Raman spectroscopy (See SI Fig. S2 for detailed phase index procedure). Although the three grains have the same out-of-plane growth direction, within the plane they orient differently, as indicated by the g (020) vectors. The angle between grain I and grain II is about 56°, and between grain II and grain III is about 45°.

In addition to examining multiple randomly transferred crystals, we performed TEM and Raman analysis on the same thicker crystal (≈ 100 nm) by breaking it into two halves. The resulted TEM index matches well with that of Raman analysis (characteristic peaks between 100 cm⁻¹ and 200 cm⁻¹), confirming that Raman spectroscopy is an accurate and rapid way to identify ultra-thin ϵ -Fe₂O₃. In total, we have checked 23 crystals with thicknesses range from 5.1 nm to 260 nm. Of these, 22 crystals show the ϵ phase (see SI Fig. S3).

To provide more insights about the growth mechanism, we analyzed the ε-Fe₂O₃ flakes by Time-of-Flight Secondary Ion Mass Spectrometry (TOF-SIMS). The chemical mapping in Fig. S4

reveals that the flakes are laterally uniform with a clear contrast between the flakes and mica substrate. A higher Cl signal in the flake regions (Fig. S4b) indicates the preferential adsorption of Cl. In-depth analysis further confirms that Cl is present on the surface of the flake, while there is no noticeable Cl inside of ε -Fe₂O₃ flake. This TOF-SIMS analysis provides evidence that the break of thermodynamic equilibrium by absorption of Cl might be one of the reasons why we can achieve highly anisotropic ultra-thin growth for ε -Fe₂O₃.

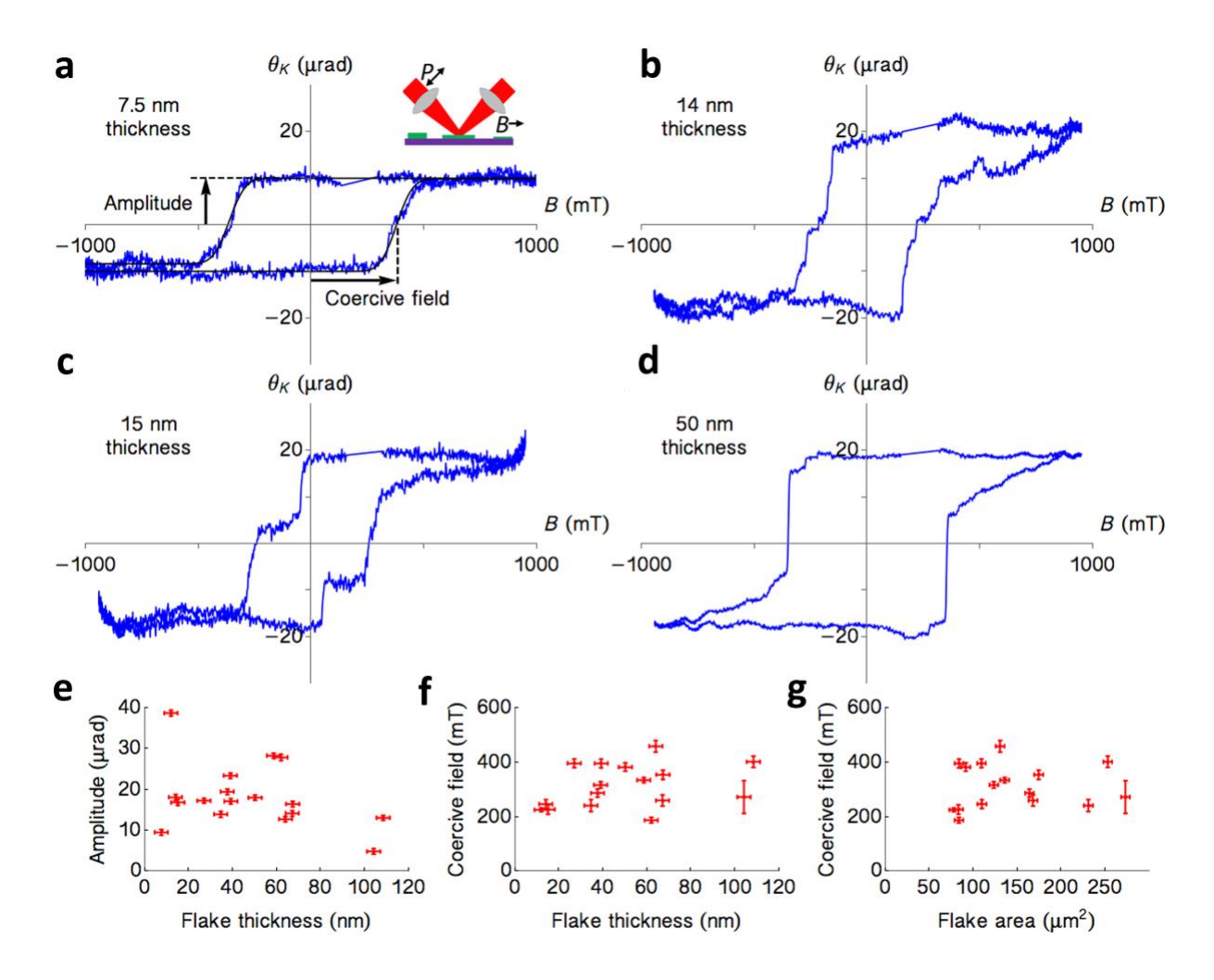


Figure 3. Room-temperature magnetic order in nanoscale thickness ϵ -Fe₂O₃. (a-d) Hysteresis loops obtained from crystals with varying thicknesses from 7.5 nm to 50.1 nm, demonstrating magnetic order with symmetric hysteresis and coercive fields \approx 300 mT. (e) The amplitude of the

Kerr effect plotted against the thickness of the crystals measured by AFM, showing no correlation. (f) The coercive field plotted as a function of thickness, showing no obvious trend. Coercive fields and amplitudes are measured from the hysteresis loops by fitting the magnetic transitions to error functions. Backgrounds were removed from these hysteresis curves according to the procedure described in Fig. S5. (g) The coercive field plotted as a function of flake area, showing no obvious trend.

We next probe the magnetic properties of these ultra-thin ε-Fe₂O₃ crystals with longitudinal MOKE measurement at room temperature (295K). The measurement geometry is shown as inset in Fig. 3a, and further details of the measurement and data processing are described in Methods. Fig. 3a-d show typical hysteresis loops of Kerr rotation θ_K as a function of magnetic field, B, for samples with thickness ranging from 7.5 nm to 50.1 nm. These loops clearly show roomtemperature magnetic order in ultra-thin ε-Fe₂O₃ with well-defined transitions, and coercive fields of hundreds of mT. Noting the difference in the amplitude of the Kerr effect, in particular between the 7.5 nm and 15 nm thick samples (Fig. 3a and Fig. 3c), we investigated 15 other crystals with different thicknesses to check for an influence of thickness on magnetic properties. Of these, all show similar room temperature switching behavior, with a mean coercive field of 290 mT and a standard deviation of 80 mT. These results agree well with previous measurements of nanoparticles $^{21-22}$ and thin films of ϵ -Fe₂O₃ 23 . To check the robustness of the magnetic properties of our samples at room temperature, we plot the coercive field and the amplitude of the magnetic transitions as a function of sample thickness, as measured by AFM. We find that neither the amplitude of the Kerr effect (Fig. 3e) nor the coercive field (Fig. 3f) correlates with

sample thickness. This absence of correlation confirms the robustness of magnetic order of this material even in ultra-thin thickness. This observation is in contrast with other magnetic samples. For example, magnetite (Fe₃O₄) films²⁴⁻²⁵ and nanoparticles²⁶ show a strong dependence of coercive field on sample dimensions. In this regard, our data on ultra-thin ϵ -Fe₂O₃ suggests its promising potential in ultra-compact information storage applications. We also plot the coercive field as a function of flake area in Fig. 3g, which also shows no correlation. These observations suggest that coercive field is set by local properties within the ϵ -Fe₂O₃, rather than by any thickness tuning of exchange processes or by geometric anisotropy.

Electronic transport measurements (see Fig. S6 and Fig. S7) show that the material is highly resistive, with a room temperature resistivity on the order of $100 \Omega \cdot m$. This is comparable to expectations for the related oxide, hematite²⁷⁻²⁸, and implies high sample quality through the lack of doping from vacancies or impurities.

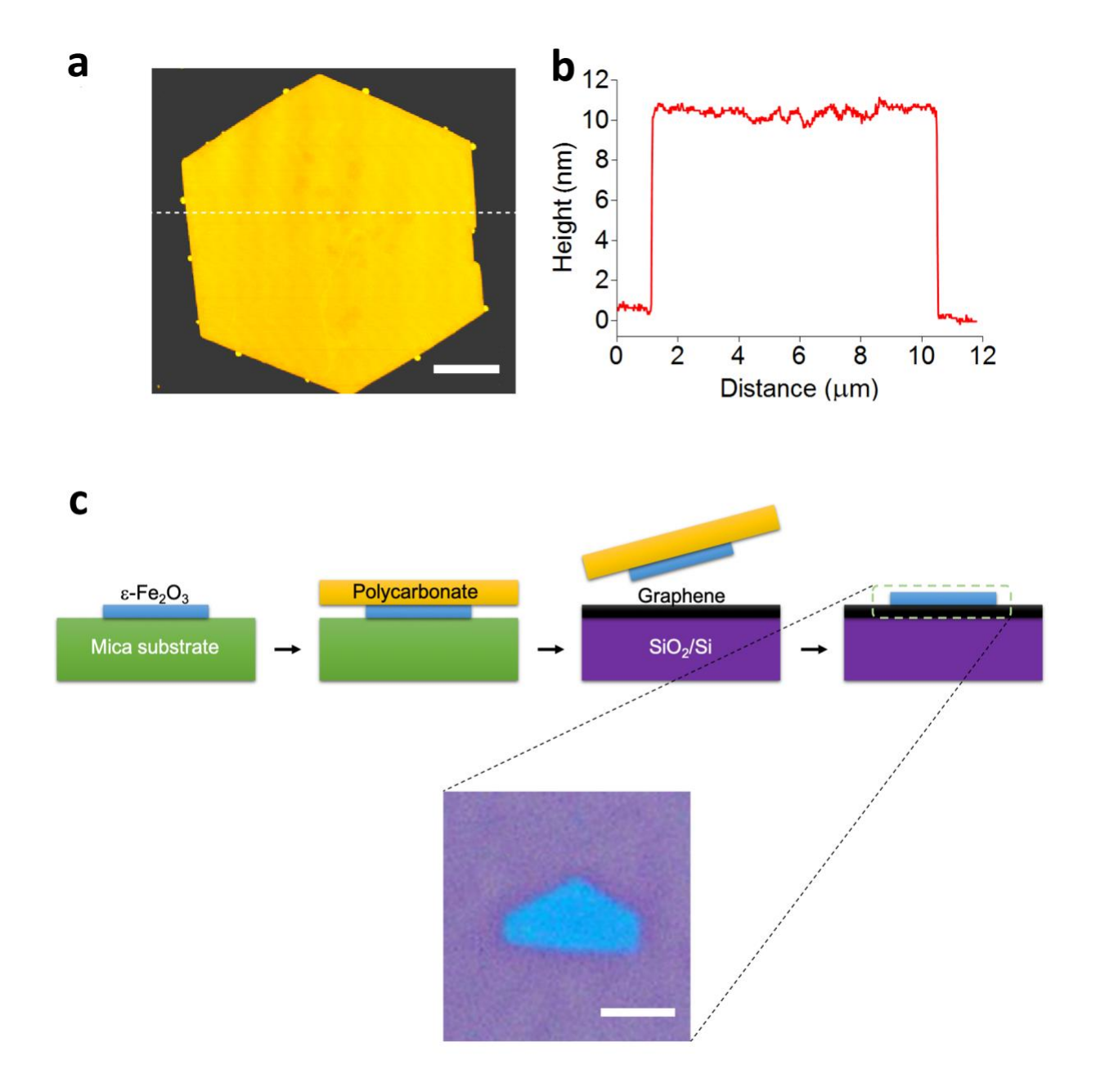


Figure 4. Stability and transferability of ultra-thin ε-Fe₂O₃. (a) AFM image of a crystal stored under ambient conditions for over three months. No obvious voids or morphology changes can be observed. Scale bar: 2 μm. (b) Height profile analysis across the whole crystal indicates that the surface is highly smooth, with a standard deviation roughness of 0.28 nm, and edges are sharp without any signs of degradation. (c) Scheme of transferring ultra-thin ε-Fe₂O₃ crystals

from mica growth substrate and building an ϵ -Fe₂O₃/graphene heterostructure. The monolayer CVD-grown graphene film is on a SiO₂/Si substrate. Scale bar: 2 μ m.

One distinctive advantage of ultra-thin ε -Fe₂O₃ is that these crystals have exceptional stability. Fig. 4a is an AFM image of a crystal stored in ambient condition (T = 24.0 °C, RH = 39%) for over three months. No obvious voids or morphology changes were observed. Height profile analyses across the whole sample (Fig. 4b) reveals that the crystal still has an atomically smooth surface with a standard deviation roughness of 0.28 nm and sharp edges. Therefore, it is not likely that these ultra-thin ε -Fe₂O₃ crystals will be further degraded, demonstrating extraordinary stability compared to other nanoscale magnetic materials reported so far. Remarkably, ultra-thin ε -Fe₂O₃ can be transferred easily from the growth substrate like van der Waals layered materials. Taking advantage of its stability, we prepared a ε -Fe₂O₃/graphene film heterostructure through a water assisted polycarbonate transfer method, where no harsh chemical etchants were involved. The transfer scheme and outcome are illustrated in Fig. 4c. The well-defined and intact flake after transfer clearly demonstrates the bonding between ε -Fe₂O₃ and its growth substrate is noncovalent, thereby allowing ultra-thin ε -Fe₂O₃ to be handled as a van der Waals material for building different types of heterostructure devices.

In summary, ultra-thin ε-Fe₂O₃ can be synthesized via a scalable ambient CVD technique. MOKE measurements on individual crystals clearly show that ultra-thin ε-Fe₂O₃ is magnetically ordered at room temperature with coercive fields of 200 to 400 mT and sharp magnetic transitions, even down to 7.5 nm thickness. Moreover, ultra-thin ε-Fe₂O₃ will not degrade under ambient conditions for months. We further demonstrate that these crystals can be transferred

from growth substrate and integrated into ε-Fe₂O₃/graphene heterostructure through well-

established methods developed for 2D materials at ambient conditions. Thanks to these useful

and unique properties, ultra-thin ε-Fe₂O₃ will be a promising and distinctive platform to explore

magnetism in the nanoscale limit. It is envisioned that new conceptual devices with novel spin

functionalities could be developed through heterostructure engineering with other layered

materials.

ASSOCIATED CONTENT

Supporting Information.

The following files are available free of charge.

Materials and Methods

Figs. S1 to S7

AUTHOR INFORMATION

Corresponding Author

* Email: jlou@rice.edu

Author Contributions

J. Y. and J. L. conceived the idea and designed the experiments. J. Y., S. P. and Q. F. conducted

the materials growth and Raman, AFM characterization. A. B. and S. C. performed the MOKE

measurements. A.B. processed and analyzed the MOKE data. H. G. carried out the TEM

12

characterization and phase index from electron diffraction patterns. X. Z. and D. N. handled the device fabrication for magnetotransport measurements. All authors wrote the manuscript and discussed the results at all stages. All authors have given approval to the final version of the manuscript. †These authors contributed equally.

Funding Sources

The CVD growth, Raman and AFM characterization of Fe₂O₃ was supported by the Welch Foundation (C-1716). TEM characterization was supported by a DOE BES grant (DE-SC0018193). MOKE measurements at the NHMFL were supported by the National Science Foundation DMR-1644779. Device fabrication and transport measurements were funded by Rice IDEA support and National Science Foundation DMR-1704264. ALB acknowledges support of the Los Alamos LDRD program.

Notes

Authors declare no competing interests.

ACKNOWLEDGMENT

We thank K. H. and L. Yang for their helpful discussion, C. Sui for assistance with TEM sample preparation, and Panpan Zhou for assistance with device fabrication. We acknowledge the support of the National Science Foundation for access to the ToF-SIMS at Rice University, supported through CBET1626418. ToF-SIMS analysis were carried out with support provided by the Shared Equipment Authority at Rice University.

REFERENCES

1. K. S. Novoselov, A. Mishchenko, A. Carvalho, A. H. Castro Neto, 2D materials and van der Waals heterostructures. *Science* **353**, aac9439 (2016).

- 2. A. K. Geim, I. V. Grigorieva, Van der Waals heterostructures. *Nature* 499, 419-425, (2013).
- 3. K. F. Mak, K. L. McGill, J. Park, P. L. McEuen, The valley Hall effect in MoS₂ transistors. *Science* **344**, 1489-1492 (2014).
- 4. K. Chang, J. Liu, H. Lin, N. Wang, K. Zhao, A. Zhang, F. Jin, Y. Zhong, X. Hu, W. Duan, Q. Zhang, L. Fu, Q. K. Xue, X. Chen, S. H. Ji, Discovery of robust in-plane ferroelectricity in atomic-thick SnTe. *Science* **353**, 274-278 (2016).
- A. Gozar, G. Logvenov, L. F. Kourkoutis, A. T. Bollinger, L. A. Giannuzzi, D. A. Muller, I. Bozovic, High-temperature interface superconductivity between metallic and insulating copper oxides. *Nature* 455, 782-785 (2008).
- 6. X. Xi, L. Zhao, Z. Wang, H. Berger, L. Forro, J. Shan, K. F. Mak, Strongly enhanced charge-density-wave order in monolayer NbSe₂. *Nat. Nanotechnol.* **10**, 765-769 (2015).
- 7. T. Ritschel, J. Trinckauf, K. Koepernik, B. Buchner, M. v. Zimmermann, H. Berger, Y. I. Joe, P. Abbamonte, J. Geck, Orbital textures and charge density waves in transition metal dichalcogenides. *Nat. Phys.* **11**, 328-331 (2015).
- 8. G. Z. Magda, X. Jin, I. Hagymasi, P. Vancso, Z. Osvath, P. Nemes-Incze, C. Hwang, L. P. Biro, L. Tapaszto, Room-temperature magnetic order on zigzag edges of narrow graphene nanoribbons. *Nature* **514**, 608-611 (2014).
- 9. H. Gonzalez-Herrero, J. M. Gomez-Rodriguez, P. Mallet, M. Moaied, J. J. Palacios, C. Salgado, M. M. Ugeda, J.-Y. Veuillen, F. Yndurain, I. Brihuega, Atomic-scale control of graphene magnetism by using hydrogen atoms. *Science* **352**, 437-441 (2016).

- 10. L. Seixas, A. Carvalho, A. H. Castro Neto, Atomically thin dilute magnetism in Co-doped phosphorene. *Phys. Rev. B* **91**, 155138 (2015).
- 11. B. Huang, G. Clark, E. Navarro-Moratalla, D. R. Klein, R. Cheng, K. L. Seyler, D. Zhong, E. Schmidgall, M. A. Mcguire, D. H. Cobden, W. Yao, D. Xiao, P. Jarillo-Herrero, X. Xu, Layer-dependent ferromagnetism in a van der Waals crystal down to the monolayer limit. *Nature* 546, 270-273 (2017).
- C. Gong, L. Li, Z. Li, H. Ji, A. Stern, Y. Xia, T. Cao, W. Bao, C. Wang, Y. Wang, Z. Q. Qiu,
 R. J. Cava, S. G. Louie, J. Xia, X. Zhang, Discovery of intrinsic ferromagnetism in two-dimensional van der Waals crystals. *Nature* 546, 265-269 (2017).
- 13. M. Bonilla, S. Kolekar, Y. Ma, H. C. Diaz, V. Kalappattil, R. Das, T. Eggers, H. R. Gutierrez, M.-H. Phan, M. Batzill, Strong room-temperature ferromagnetism in VSe₂ monolayers on van der Waals substrates. *Nat. Nanotechnol.* **13**, 289-293 (2018).
- 14. T. Song, X. Cai, M. W.-Y. Tu, X. Zhang, B. Huang, N. P. Wilson, K. L. Seyler, L. Zhu, T. Taniguchi, K. Watanabe, M. A. McGuire, D. H. Cobden, D. Xiao, W. Yao, X. Xu, Giant tunneling magnetoresistance in spin-filter van der Waals heterostructures. *Science* 360, 1214-1218 (2018).
- 15. D. R. Klein, D. MacNeill, J. L. Lado, D. Soriano, E. Navarro-Moratalla, K. Watanabe, T. Taniguchi, S. Manni, P. Canfield, J. Fernandez-Rossier, P. Jarillo-Herrero, Probing magnetism in 2D van der Waals crystalline insulators via electron tunneling. *Science* 360, 1218-1222 (2018).

- 16. Y. Deng, Y. Yu, Y. Song, J. Zhang, N. Z. Wang, Z. Sun, Y. Yi, Y. Z. Wu, S. Wu, J. Zhu, J. Wang, X. H. Chen, Y. Zhang, Gate-tunable room-temperature ferromagnetism in two-dimensional Fe₃GeTe₂. *Nature* 563, 94-99 (2018).
- 17. Z. Fei, B. Huang, P. Malinowski, W. Wang, T. Song, J. Sanchez, W. Yao, D. Xiao, X. Zhu, A. F. May, W. Wu, D. H. Cobden, J.-H. Chu, X. Xu, Two-dimensional itinerant ferromagnetism in atomically thin Fe₃GeTe₂. *Nat. Mater.* **17**, 778-782 (2018).
- A. P. Balan, S. Radhakrishnan, C. F. Woellner, S. K. Sinha, L. Deng, C. Reyes, B. M. Rao, M. Paulose, R. Neupane, A. Apte, V. Kochat, R. Vajtai, A. R. Harutyunyan, C.-W. Chu, G. Costin, D. S. Galvao, A. A. Marti, P. A. van Aken, O. K. Varghese, C. S. Tiwary, A. Ramaswamy lyer, P. M. Ajayan, Exfoliation of a non-van der Waals material from iron ore hematite. *Nat. Nanotechnol.* 13, 602-609 (2018).
- 19. J. Tucek, R. Zboril, A. Namai, S. Ohkoshi, Epsilon-Fe₂O₃: an advanced nanomaterial exhibiting giant coercive field, millimeter-wave ferromagnetic resonance, and magnetoelectric coupling. *Chem. Mater.* **22**, 6483-6505 (2010).
- 20. J. Lopez-Sanchez, A. Serrano, A. Del Campo, M. Abuin, O. Rodriguez de la Fuente, N. Carmona, Sol-gel synthesis and micro-Raman characterization of epsilon-Fe₂O₃ micro- and nanoparticles. *Chem. Mater.* **28**, 511-518 (2016).
- 21. J. Jin, S. Ohkoshi, K. Hashimoto, Giant coercive field of nanometer-sized iron oxide. *Adv. Mater.* **16**, 48-51 (2004).
- 22. E. Taboada, M. Gich, A. Roig, Nanospheres of silica with an epsilon-Fe₂O₃ single crystal nucleus. *ACS Nano* **3**, 3377-3382 (2009).

- 23. M. Gich, J. Gazquez, A. Roig, A. Crespi, J. Fontcuberta, J. C. Idrobo, S. J. Pennycook, M. Varela, V. Skumryev, M. Varela, Epitaxial stabilization of epsilon-Fe₂O₃ (00l) thin films on SrTiO₃ (111). *Appl. Phys. Lett.* **96**, 112508 (2010).
- 24. J.-B. Moussy, S. Gota, A. Bataille, M.-J. Guittet, M. Gautier-Soyer, F. Delille, B. Dieny, F. Ott, T. D. Doan, P. Warin, P. Bayle-Guillemaud, C. Gatel, E. Snoeck, Thickness dependence of anomalous magnetic behavior in epitaxial Fe₃O₄(111) thin films: Effect of density of antiphase boundaries. *Phys. Rev. B* **70**, 174448 (2004).
- 25. D. T. Margulies, F. T. Parker, F. E. Spada, R. S. Goldman, J. Li, R. Sinclair, A. E. Berkowitz, Anomalous moment and anisotropy behavior in Fe₃O₄ films. *Phys. Rev. B* **53**, 9175-9187 (1996).
- 26. G. F. Goya, T. S. Berquo, F. C. Fonseca, M. P. Morales, Static and dynamic magnetic properties of spherical magnetite nanoparticles. *Jour. Appl. Phys.* **94**, 3520-3528 (2003).
- 27. F. J. Morin, Electrical properties of □-Fe₂O₃ and □-Fe₂O₃ containing titanium. *Phys. Rev.*83, 1005 (1951).
- 28. J. A. Glasscock, P. R. F. Barnes, I. C. Plumb, A. Bendavid, P. J. Martin, Structural, optical and electrical properties of undoped polycrystalline hematite thin films produced using filtered arc deposition. *Thin Solid Films* **516**, 1716-1724 (2008).

TABLE OF CONTENTS GRAPHIC

